

Article

Nanoindentation Investigation on the Size-Dependent Creep Behavior in a Zr-Cu-Ag-Al Bulk Metallic Glass

Z. Y. Ding ^{1,2}, Y. X. Song ^{1,2}, Y. Ma ^{1,*}, X. W. Huang ¹ and T. H. Zhang ^{3,*} 

¹ College of Mechanical Engineering, Zhejiang University of Technology, Hangzhou 310014, China; zyding@zjut.edu.cn (Z.Y.D.); songyux@zjut.edu.cn (Y.X.S.); huangxw@zjut.edu.cn (X.W.H.)

² Institute of Process Equipment and Control Engineering, Zhejiang University of Technology, Hangzhou 310014, China

³ Institute of Solid Mechanics, Beihang University, Beijing 100191, China

* Correspondence: may@zjut.edu.cn (Y.M.); zhangth66@buaa.edu.cn (T.H.Z.); Tel.: +86-571-88320132 (Y.M. & T.H.Z.)

Received: 1 May 2019; Accepted: 23 May 2019; Published: 27 May 2019



Abstract: Nanoindentation technology has been widely adopted to study creep behavior in small regions. However, nanoindentation creep behavior of metallic glass is still not well understood. In the present work, we investigated nanoindentation size effects on creep deformation in a Zr-based bulk metallic glass at room temperature. The total creep strain and strain rate of steady-state creep were gradually decreased with increasing holding depth under a Berkovich indenter, indicating a length-scale-dependent creep resistance. For a spherical indenter, creep deformations were insignificant in elastic regions and then greatly enhanced by increasing holding strain in plastic regions. Strain rate sensitivities (SRS) decreased with increasing holding depth and holding strain at first, and then stabilized as holding depth was beyond about 500 nm for both indenters. SRS values were 0.4–0.5 in elastic regions, in which atomic diffusion and free volume migration could be the creep mechanism. On the other hand, evolution of the shear transformation zone was suggested as a creep mechanism in plastic regions, and the corresponding SRS values were in the range of 0.05 to 0.3.

Keywords: metallic glass; nanoindentation; creep; size effect; strain rate sensitivity

1. Introduction

As a relatively new member of the glass family, metallic glasses have great potential to be an excellent candidate as engineering materials due to their attractive mechanical properties, such as super high yield strength, large elastic limit (~2%), and strong wear resistance [1–3]. Nevertheless, the brittleness inherited from the amorphous structure seriously hinders the commercial application of bulk metallic glasses [4]. Distinct to the dislocation move in crystalline alloys, plastic mechanism in metallic glass is still under debate and on the cutting edge of structure investigations [5,6]. In recent years, size effect on mechanical properties of metallic glass has attracted numerous attention [7–9]. By reducing physical dimensions, ductility could be greatly enhanced at the nanoscale without sacrificing high strength. Nanoindentation is the most powerful technology to use to study mechanical properties in small regions, which has been widely used to reveal the size effect in metals and alloys [10].

Creep is a time-dependent plastic deformation, which is an inevitable process and vital to engineering materials on service [11]. Relying on nanoindentation, creep behaviors can be studied at small region, ignoring the limitation of required standard size in conventional creep test [12–14]. For metallic glass, creep resistance is not fully studied and creep mechanism is far from being understood [15,16]. In order to avoid undesired influence by thermal drift, the nanoindentation

creep test is commonly conducted at low temperatures. The sample size effect on creep deformation has also been examined by nanoindentation. Yoo et al. studied room-temperature creep behavior in metallic glass nanopillars with 250~2000 nm diameter by elastic holding [17]. As with most nanoindentation creep experiments, creep behaviors were detected in plastic regions by adopting a three-sided pyramidal, namely a Berkovich indenter. Wang et al. performed creep tests in Cu-Zr films with thicknesses from 1000 to 3000 nm [18], while Ma et al. investigated creep behaviors in 500–1500 nm Cu-Zr-Al films [19]. Creep features in Ni-Nb thin films and ribbons were also compared by Ma [20]. Under both elastic and plastic holdings, creep deformation was more pronounced in smaller samples. That is to say, the creep feature seems to be in conflict with the “smaller is stronger” principle in metallic glass.

On the other hand, the size effect on creep deformation could also be studied by changing the nanoindentation holding depth. In this scenario, the creep feature is linked to the deformation volume beneath an indenter whilst the inner structure state is unchanged. Superficially, in previous reports, the recorded creep displacements were increased with holding depth under both Berkovich and spherical indenters [21–24]. This phenomenon was commonly attributed to the more excess free volume generated in deep nanoindentation. In fact, it is conceivable that creep displacement is in proportion to the length scale of the sample and holding strain in conventional uniaxial holding. Therefore, true creep resistance needs to be carefully examined in metallic glass and linked to deformation volume and holding strain during nanoindentation holding. In the present work, we aim to reveal the intrinsic nanoindentation size effect on creep deformation in a Zr-Cu-Ag-Al metallic glass. By adopting a standard Berkovich indenter, creep deformation can be studied at various depths while the holding strain is constant. Using a spherical indenter, the holding strain effect on creep deformation could be investigated.

2. Materials and Methods

Zr₄₆Cu_{37.6}Ag_{8.4}Al₈ alloy ingots were prepared from high pure elements (99.99%) by arc mixing in a Ti-gettered argon atmosphere. Alloy sheets with a rectangular cross-section of 2 mm × 30 mm were obtained by injecting alloy melt into a copper mold. Prior to nanoindentation, the specimen surface was precisely polished to a mirror finish. The structure of the as-cast Zr-Cu-Ag-Al specimen was detected using X-ray diffraction (XRD) with Cu K α radiation. By means of X-ray energy dispersive spectrometer (EDS) attached on a SEM, the chemical composition was detected, which was equal to the alloy ingot.

Nanoindentation creep tests were conducted at a constant temperature of 20 °C on Agilent Nano Indenter G200. The displacement and load resolutions of the machine are 0.01 nm and 50 nN, respectively. Constant-load holding method was adopted, during which displacement of indenter into the surface at a prescribed load could be continuously recorded. A standard Berkovich indenter and a spherical indenter with a nominal radius of 20 μ m were used, respectively. Upon calibration on fused silica, the true contact radius of spherical indenter was obtained as 9.8 μ m. The Berkovich indenter was held at maximum loads of 5, 10, 25, 50, 100, 200, and 400 mN. For spherical nanoindentation, the peak loads were 2, 5, 10, 30, 60, 120, 200, 300, 470, and 700 mN. The loading rate and holding time were fixed, equal to 2 mN/s and 500 s. More than twenty-five independent measurements were performed under each testing condition. All the nanoindentation tests were carried out until thermal drift reduced to below 0.02 nm/s, and drift correction was strictly performed at 10% of the maximum load during the unloading process. Upon drift correction, the thermal drift effect could be greatly alleviated, especially for creep displacement during the holding stage.

3. Results and Discussion

Figure S1 shows the typical X-ray diffraction pattern of the as-prepared Zr-Cu-Ag-Al alloy. It is clear that only a broad diffraction peak can be detected, which represents a crystal free structure. The representative creep load versus displacement (P - h) curves at various holding loads under a

Berkovich indenter are exhibited in Figure 1a. The P - h curves at shallow depths were enlarged, as shown in the insets. The permanent displacement, i.e., creep flow, could be observed in the holding stage, though it was subtle particularly under small loads. As exhibited in Figure 1b, the creep displacement during the holding stage was plotted as a function of holding time. For a clear view, the onsets of both x -axis (holding time) and y -axis (displacement) in graph were set to zero. The creep P - h curves and creep flow curves under spherical indenter were similar to those under Berkovich indenter, as exhibited in Figure S2 in the Supplementary Materials. For both indenters, creep displacement was more pronounced at larger holding loads and/or depths.

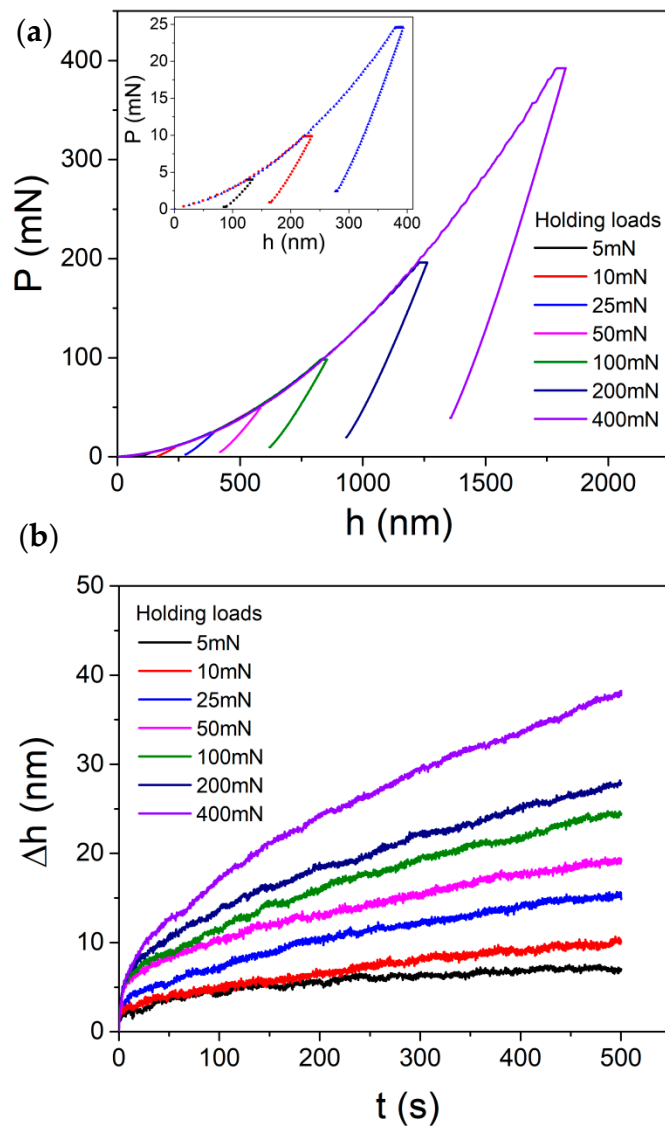


Figure 1. (a) The typical creep P - h curves at various holding depths under Berkovich indenter. P - h curves at shallow depths were enlarged in the inset. (b) Creep displacements at various holding loads were plotted with holding time.

The total creep displacements at the end of the holding stage were recorded, which were plotted with holding depths, as shown in Figure 2. The creep displacement in the Berkovich nanoindentation was increased with holding depth, while in spherical nanoindentation, creep displacement was almost independent of holding depth at first and then quickly increased. Creep deformations under Berkovich indenter were more pronounced than those under spherical indenter. The holding-depth-facilitated nanoindentation creep displacements were consistent with previous reports in metallic glasses.

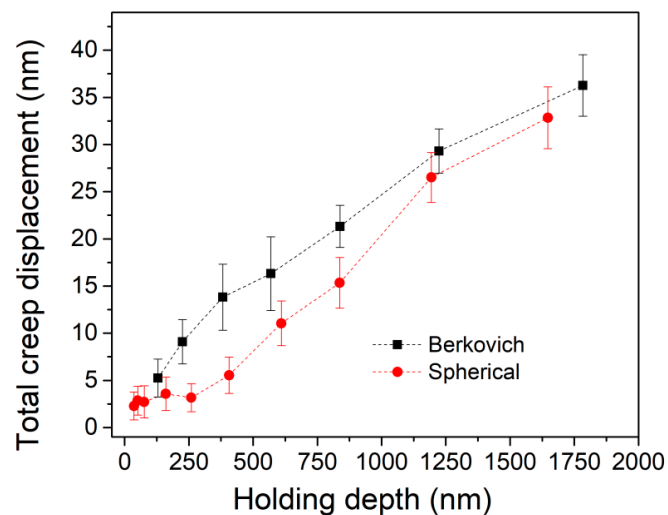


Figure 2. The total creep displacements in the end of holding stage were plotted with holding depth for both indenters.

For a standard Berkovich indenter (without tip bluntness), the imposed plastic volume and stress distribution during nanoindentation are self-similar at various pressed depths. Nanoindentation strains at various holding depths were constant, equal to 7.1% ($0.2\cot 70.5^\circ$). Theoretically, creep displacement under a Berkovich indenter would be in proportion to the holding depth whilst creep strain would be invariable, regardless of structure agitation at various holding depth. Furthermore, the anticipation that more excess free volume could be generated at deep nanoindentation lacks strict verification, while for a spherical indenter, the deformation zone gradually evolved from elastic to elastoplastic with increasing pressed depth. The nanoindentation strain was continuously increased to the limit about 11% (the configuration of spherical indenter is a conical body with spherical tip, the maximum indentation strain would be approaching to 11% by $0.2\cot 61^\circ$). Under spherical nanoindentation, more severe structural agitation and better atomic mobility could be expected due to the increased plastic strain at deeper location. Thus, the situation under spherical indenter was more complicated than that under a Berkovich indenter. The increased creep displacement could be attributed to the combined effects of deformation volume, holding strain, and atomic mobility. The creep deformation under spherical indenter needs to be discussed separately at elastic and plastic holdings.

According to Bei's work [25], the first pop-in event on the loading sequence could be linked to incipient plasticity. Figure 3a shows the typical spherical P - h curve at 200 mN (holding time was 5 s) with loading rate of 2 mN/s. The pop-in events with length scales of 20~30 nm clear occurred, which represent the generation of shear bands. The initial loading sequence could be well fitted by the Hertzian elastic contact equation [26], given by

$$P = \frac{4}{3}E_r \sqrt{R}h^{1.5} \quad (1)$$

where E_r is the reduced elastic modulus which accounts for the elastic displacement occurred in both the tip and sample, given by

$$\frac{1}{E_r} = \frac{1 - \nu_i^2}{E_i} + \frac{1 - \nu_s^2}{E_s} \quad (2)$$

where E and ν are the elastic modulus and Poisson's ratio, and the subscripts s and i represent the sample and the indenter, respectively. For commonly used diamond tip, $E_i = 1141$ GPa and $\nu_i = 0.07$. For the Zr-Cu-Ag-Al metallic glass, elastic modulus was measured as 110 GPa as shown in Figure S3 in the Supplementary Materials and the Poisson's ratio is 0.36 [27]. The Hertzian fitting line deviated from the P - h curve at the position of the first pop-in. This clearly indicates the transition from elastic

deformation to plastic deformation once the first pop-in emerges. Shear banding nucleation in metallic glass is a stochastic process, which could result in a scatter distribution of the first pop-in event [28]. By conducting 81 measurements at a 9×9 matrix at intervals of $50 \mu\text{m}$, the critical loads at first pop-in events were detected to be uniformly scattered in the range between 90 and 150 mN, as shown in the inset of Figure 3a. Thus, 2–60 mN holdings were at elastic regions and 200–700 mN holdings were at plastic regions under spherical indenter. The 120 mN holding was exactly around the yielding point of Zr-Cu-Ag-Al sample. We can regard approximately 120 mN holding as the elastic holding because plastic deformation was still negligible. The holding strains at various holding depths were estimated for spherical indenter by $\varepsilon_i = 0.2(\alpha/R)$, α is the contact radius. As exhibited in Figure 3b, the holding strain increased from 1.2% to 10% as peak load increased from 2 to 700 mN. The elastic limit under $9.8 \mu\text{m}$ spherical indenter was about 4%, which was far beyond the typical $\sim 2\%$ for bulk metallic glasses. This could be explained from the complicated stress distribution beneath the indenter where incipient plasticity is unable to be triggered immediately when the maximum stress attains yield stress [29]. To form a shear band during nanoindentation, there needs a certain space along the shear path of which stress has been beyond the yield stress.

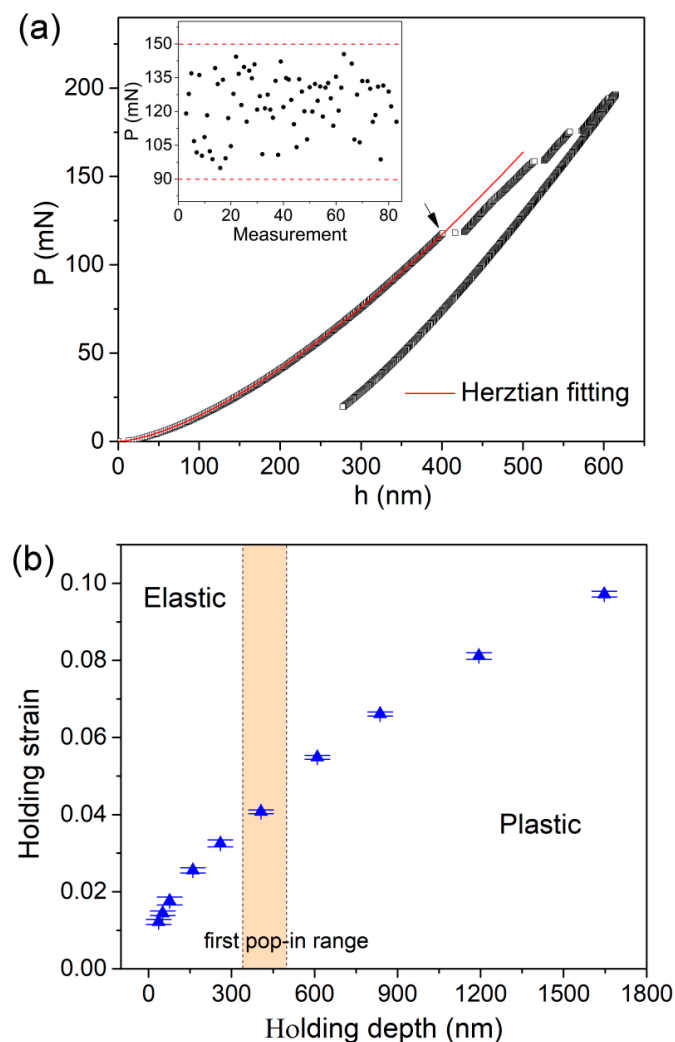


Figure 3. (a) The typical $P-h$ curve under 200 mN spherical indenter with 5 s holding. The distribution range of the critical load at the first pop-in event is shown in the inset, which was plotted with measurement. (b) The corresponding holding strain for each holding load was calculated for spherical nanoindentation and was plotted with holding depth. The creep tests could be divided as elastic holding and plastic holding.

For creep deformation under Berkovich indenter, we defined creep strain as $\Delta h/h_c$, in which Δh is the total creep displacement and h_c is the contact displacement at the beginning of holding stage. Contact displacement was estimated by $h_c = h - \varepsilon \times P/S$, in which $\varepsilon = 0.72$, S is the stiffness deduced from the unloading curve. The creep strain rate of steady-state part was estimated by $\dot{\varepsilon} = \frac{1}{h_c} \frac{dh_c}{dt}$. The mean value of creep strain rate at the last 200 s segment of holding stage was adopted. Figure 4a exhibits creep strain and strain rate of steady-state creep under Berkovich indenter at various holding depths. The creep strain was continuously decreased from 0.04 to 0.02 with increasing holding depth from 130 to 1780 nm. Meanwhile, creep strain rate decreased from 1.1×10^{-4} to $5.4 \times 10^{-5} \text{ s}^{-1}$. That is to say, creep deformation was actually depressed with increasing nanoindentation depth under a Berkovich indenter. This result confirms previous reports about sample-size-dependent creep flow [17–20]. From the perspective of structure agitation, the density of shear bands could be decreased at deep nanoindentation, i.e., lower density of excess free volume. On the other hand, size effect on plastic deformation has been largely reported in metallic glass that plastic flow is facilitated at the nanoscale [7–9], which suggests a better atomic mobility. Therefore, the enhanced creep deformation at shallow depth under a Berkovich indenter could be explained qualitatively.

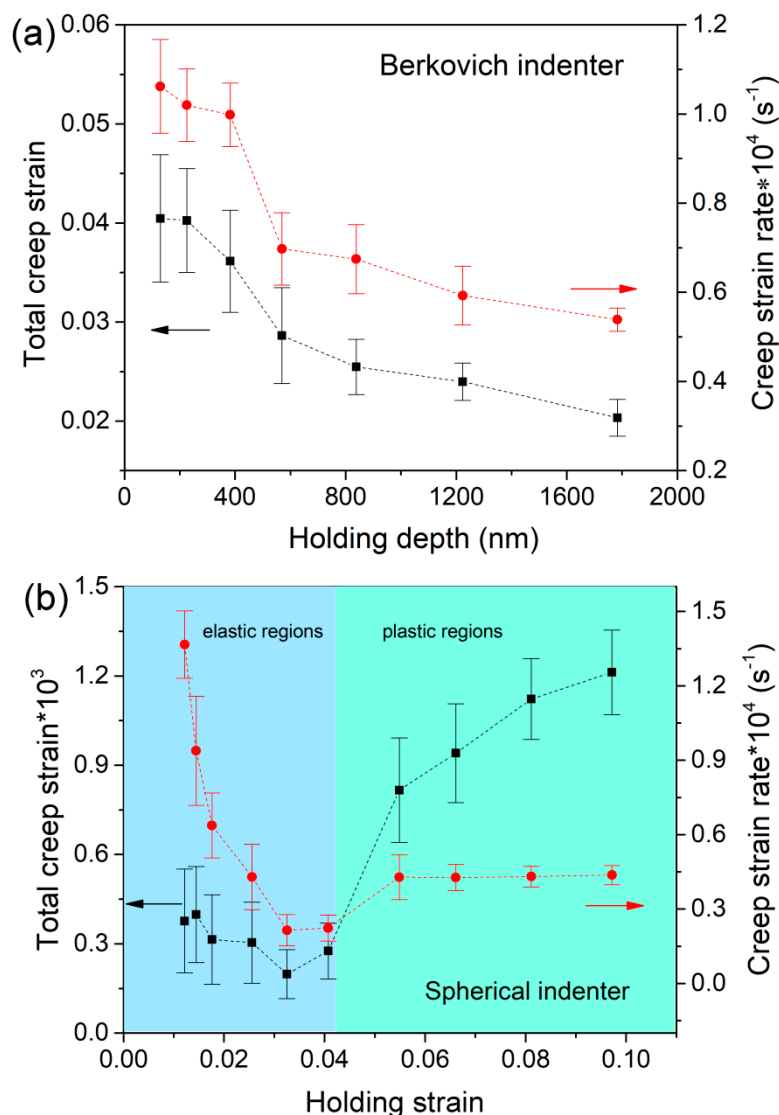


Figure 4. The total creep strain in the end of holding stage and strain rate of steady-state creep were estimated for (a) Berkovich and (b) spherical indenters, which were plotted with holding depth and holding strain.

Creep strain under spherical indenter was calculated by $0.2(\alpha - \alpha_0)/R$, where a and a_0 are the contact radii at the beginning and ending of holding stage, respectively. Creep strain rate was calculated by $\dot{\epsilon} = \frac{1}{\sqrt{A}} \frac{d\sqrt{A}}{dt}$, where A is the contact area, equal to $2\pi R h_c$ at plastic region and $\pi R h$ at elastic region. Figure 4b depicts the correlations between creep strain, creep strain rate, and holding strain under spherical indenter. At elastic regions, creep strains were insignificant (lower than 0.04%) and slightly decreased as increasing holding strain. It is rational that creep flow hardly occurred under elastic holding at room temperature for the high-melting bulk metallic glass in such short duration (compared to conventional creep measurement). The present result indicates that creep deformation at elastic region is mainly dependent on structure state, rather than holding strain. Atomic diffusion on the contact surface and the migration of pre-existing free volume could be the creep mechanism at elastic holdings. As the holding strain turned to plastic, a sudden increase of creep strain was observed. At plastic regions, creep strain was greatly increased from about 0.04% to 0.1% as holding strain increased from 4% to 10%. For plastic holdings, the evolution of shear transformation zone (STZ) dominated during creep deformation. With increasing holding strain, plastic zone beneath indenter increased and more STZs were activated to carry creep flow. In this scene, the increased plastic strain and more severe structure agitation jointly stimulated creep deformation as increasing holding strain. On the other hand, creep strain rate precipitously decreased as increasing holding strain at elastic regions and was independent on holding strain at plastic regions. As holding strain increased from elastic to plastic, the enlargement of creep strain rate was apparently less dramatic than the increase of creep strain. The unexpected high creep strain rates at shallow depths below 100 nm (2–10 mN holdings) were mysterious, probably due to the thermal drift effect on such weak creep deformations. Furthermore, it was indicated that steady-state creep deformation was holding-depth-independent at plastic regions, which represented the true creep resistance.

The present creep feature under nanoindentation was similar to conventional testing. Hence, it has merits to estimate strain rate sensitivity (SRS) in order to reveal the creep mechanism and its correlation with nanoindentation length scale. Here, we selected 200 mN-holding testing by spherical indenter as an illustration to calculate SRS. As exhibited in Figure 5a, creep curve could be perfectly fitted ($R^2 > 0.99$) by an empirical law:

$$h(t) = h_0 + a(t - t_0)^b + kt \quad (3)$$

where h_0 , t_0 are the displacement and time at the beginning of holding stage, a , b , k are the fitting constants. The value of SRS exponent m can be evaluated via

$$m = \frac{\partial \ln \sigma}{\partial \ln \dot{\epsilon}} \quad (4)$$

The creep flow stress σ can be obtained from the mean pressure P_m beneath indenter via Tabor's mode, $P_m = 3\sigma$ [30] in the elastic region, $P_m = \frac{P}{\pi R h}$. At plastic region, the mean pressure is also defined as hardness, which is $H = \frac{P}{2\pi R h_c}$ for spherical tip and $H = \frac{P}{C h_c^2}$ for standard Berkovich indenter. C is the tip area coefficient for Berkovich indenter and was rectified upon testing on standard fused silica, equal to 24.3 here. $\dot{\epsilon}$ is the creep strain rate. Figure 5b,c show the changes of strain rate and hardness during holding stage, which were deduced from the fitting line of creep curve. Figure 5d shows the Logar-Logar correlation between hardness and strain rate during the holding stage. Then SRS can be obtained by linearly fitting on the part of steady-state creep.

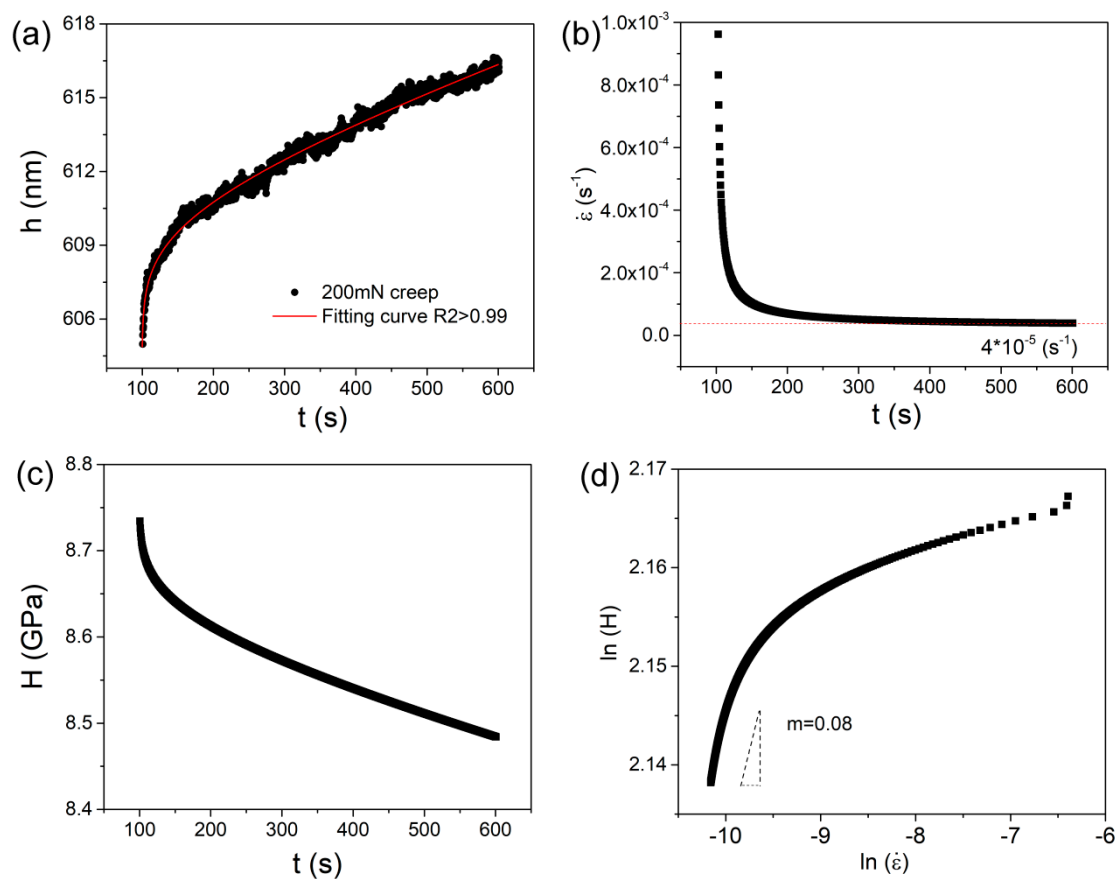


Figure 5. (a) The creep displacements versus holding time, which is perfectly fitted by an empirical law; (b) the creep strain rate versus holding time; (c) the hardness versus holding time; (d) the log–log correlation between hardness and strain rate obtained from the creep, strain rate sensitivity was estimated by linear fitting of the steady-state part.

Figure 6a shows the correlation between m and holding depth for Berkovich indenter. SRS was decreased from 0.17 to 0.075 as holding depth increased from 130 to 570 nm, and then tended to stabilize around 0.07. In the present work, the tip bluntness effect on creep behavior at shallow depth could be excluded since the minimum pressed depth was beyond 100 nm. Figure 6b shows the correlation between m and holding strain for spherical indenter. At elastic regions, m greatly decreased from 0.53 to 0.16, as holding strain increased from 1.2% to 4%. At plastic regions, m slightly decreased, from 0.09 to 0.055, as holding strain increased from 5.5% to 10%. Apparently, SRS decreased with increasing holding depth and settled as the pressed depth was larger than about 500 nm for both indenters.

The value of strain rate sensitivity m or stress exponent n ($n = 1/m$) is widely used as an indication to creep mechanism in crystalline alloy or metals [31]. For example, dislocation move is dominating in creep flow as m falls in the range between 0.1 and 0.3. In metallic glasses, free volume generation and annihilation, shear transformation zone (STZ) evolution and atomic diffusion (under elastic contact) are thought to be the possible creep mechanisms [23], while the relationship between m and creep mechanism in metallic glass is inconclusive. For creep flow under a Berkovich indenter, the STZ creep flow could be mainly actuated by STZ evolution. The gentle change of m was probably due to that STZ size and density were also changed with nanoindentation depth. For spherical nanoindentation creep, it is worth mentioning that m was in between 0.25 and 0.055 within holding strain range from 2.6% to 10%. It is reasonable that m at plastic region under spherical indenter was much comparable to Berkovich nanoindentation, due to the same creep mechanism, while for 30–120 mN elastic holdings (2.6–4% holding strains), the maximum stress beneath indenter had already exceeded yield stress as it was aforementioned. Though it could not meet the requirement of shear banding generation,

the stress level and atomic surrounding were satisfied for STZ activation [23]. Creep deformation beneath indenter was prone to occur at the region that suffered high stress. Thus, STZ evolution might also be the creep mechanism under the nominal elastic holding at 30–120 mN. The 2–10 mN holdings, of which holding strains were below 2%, could be regarded as purely elastic under nanoindentation. In this scenario, STZs were unable to be activated. Atomic diffusion and free volume migration could be suggested as creep mechanism. Accordingly, the high values of SRS (0.4–0.5) at shallow depths under spherical indenter could be explained by the transition of creep mechanism. In the current work, we investigated creep behavior and its correlation with nanoindentation length scale and holding strain. Relying on the suggested modes for plastic deformation in metallic glass, we bridged the connection between creep mechanisms and SRS values at elastic holding and plastic holding.

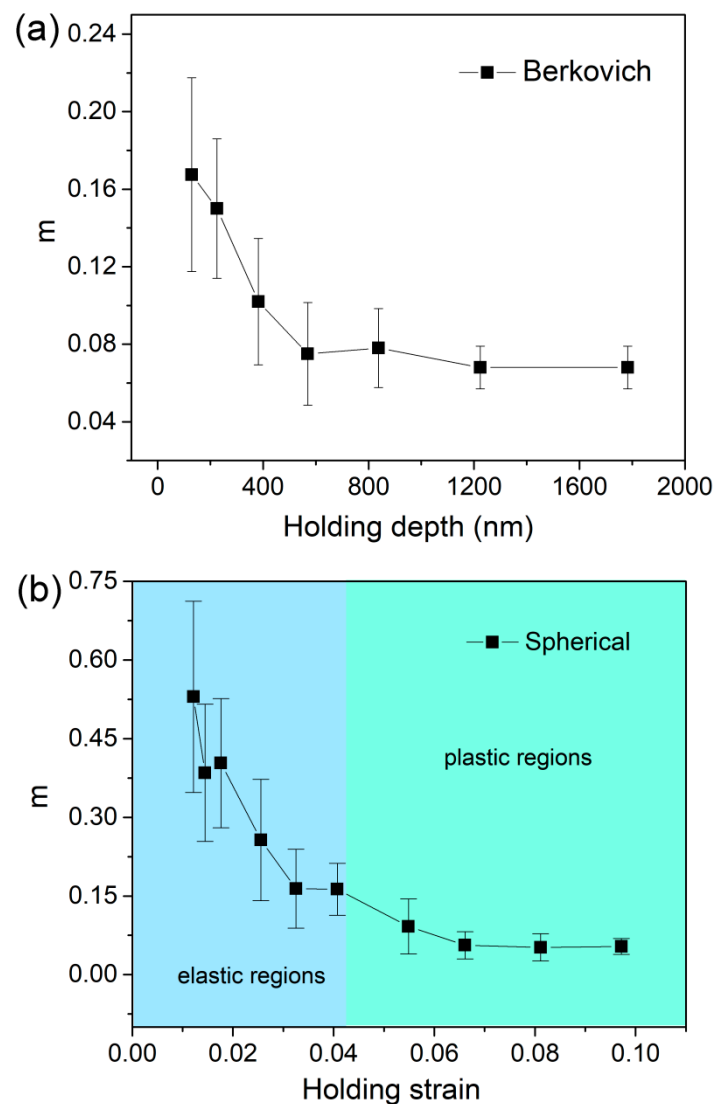


Figure 6. Strain rate sensitivities were plotted with holding depth for (a) a Berkovich indenter and plotted with holding strain for (b) a spherical indenter.

4. Conclusions

In summary, we systematically studied nanoindentation size effect on the creep deformation of a Zr-based metallic glass upon a standard a Berkovich indenter and a spherical indenter. At a given holding strain ~7.1%, creep deformation decreased with increasing holding depth, which suggested a size-dependent creep resistance. In the elastic regions, creep deformation was insignificant and weakly

decreased with holding depth. In the plastic regions, creep deformation was evidently enlarged and increased with holding strain. The estimated strain rate sensitivities (SRS) were decreased at first and then tended to stabilize with increasing holding depth and holding strain. The evolution of the shear transformation zone was presumed as a creep flow carrier in those tests with a holding strain larger than 2%. The corresponding values of SRS for STZ evolution were approximately between 0.05 and 0.3. Atomic diffusion and free volume migration were thought to be the creep mechanism at purely elastic holdings, and the characteristic values of SRS were 0.4~0.5.

Supplementary Materials: The following are available online at <http://www.mdpi.com/2075-4701/9/5/613/s1>, Figure S1: The typical XRD pattern of as-cast Zr-Cu-Ag-Al alloy, Figure S2: (a) The typical creep P - h curves at various holding depths under spherical indenter. P - h curves at shallow depths are enlarged in the inset. (b) Creep displacements at various holding loads were plotted with holding time, Figure S3: Elastic modulus was measured by continuous stiffness module (CSM) and was depicted as a function of displacement. The mean elastic modulus was 110 GPa.

Author Contributions: Data curation, Y.X.S.; formal analysis, Y.X.S.; investigation, Y.M.; software, X.W.H.; supervision, T.H.Z.; writing—original draft, Y.M.; funding acquisition, Z.Y.D.; writing—review and editing, Z.Y.D.

Funding: This research was funded by the National Natural Science Foundation of China (11727803, 11672356, 51705457) and Zhejiang Provincial Natural Science Foundation of China (LY18E010006).

Conflicts of Interest: The authors declare no conflict of interest.

References

- Inoue, A.; Shen, B.; Koshihara, H.; Kato, H.; Yavari, A.R. Cobalt-based bulk glassy alloy with ultrahigh strength and soft magnetic properties. *Nat. Mater.* **2003**, *2*, 661–663. [[CrossRef](#)]
- Jun, W.K.; Willens, R.H.; Duwez, P.O.L. Non-crystalline structure in solidified gold–silicon alloys. *Nature* **1960**, *187*, 869–870.
- Schuh, C.A.; Hufnagel, T.C.; Ramamurty, U. Mechanical behavior of amorphous alloys. *Acta Mater.* **2007**, *55*, 4067–4109. [[CrossRef](#)]
- Loffler, J.F. Bulk metallic glasses. *Intermetallics* **2003**, *11*, 529–540. [[CrossRef](#)]
- Argon, A.S. Plastic deformation in metallic glasses. *Acta Metall.* **1979**, *27*, 47–58. [[CrossRef](#)]
- Mayr, S.G. Activation energy of shear transformation zones: A key for understanding rheology of glasses and liquids. *Phys. Rev. Lett.* **2006**, *97*, 195501. [[CrossRef](#)] [[PubMed](#)]
- Jang, D.; Greer, J.R. Transition from a strong-yet-brittle to a stronger-and-ductile state by size reduction of metallic glasses. *Nat. Mater.* **2010**, *3*, 215–219. [[CrossRef](#)]
- Guo, H.; Yan, P.F.; Wang, Y.B.; Tan, J.; Zhang, Z.F.; Sui, M.L.; Ma, E. Tensile Ductility and Necking of Metallic Glass. *Nat. Mater.* **2007**, *10*, 735–739. [[CrossRef](#)]
- Ma, Y.; Cao, Q.P.; Qu, S.X.; Jiang, J.Z. Stress-state-dependent deformation behavior in Ni–Nb metallic glassy film. *Acta Mater.* **2012**, *60*, 4136–4143. [[CrossRef](#)]
- Schuh, C.A. Nanoindentation studies of materials. *Mater. Today* **2006**, *9*, 32–40. [[CrossRef](#)]
- Nabarro, F.R. Creep in commercially pure metals. *Acta Mater.* **2006**, *54*, 263–295. [[CrossRef](#)]
- Ma, Y.; Peng, G.J.; Wen, D.H.; Zhang, T.H. Nanoindentation creep behavior in a CoCrFeCuNi high-entropy alloy film with two different structure states. *Mat. Sci. Eng. A* **2015**, *621*, 111–117. [[CrossRef](#)]
- Ma, Y.; Feng, Y.H.; Debela, T.T.; Zhang, T.H. Nanoindentation study on the creep characteristics of high-entropy alloy films: Fcc versus bcc structures. *Int. J. Refract. Met. H* **2016**, *54*, 395–400. [[CrossRef](#)]
- Chen, H.; Zhang, T.H.; Ma, Y. Effect of Applied Stress on the Mechanical Properties of a Zr-Cu-Ag-Al Bulk Metallic Glass with Two Different Structure States. *Materials* **2017**, *10*, 711. [[CrossRef](#)] [[PubMed](#)]
- Zhang, T.H.; Ye, J.H.; Feng, Y.H.; Ma, Y. On the spherical nanoindentation creep of metallic glassy thin films at room temperature. *Mat. Sci. Eng. A* **2017**, *685*, 294–299. [[CrossRef](#)]
- Ma, Y.; Ye, J.H.; Peng, G.J.; Zhang, T.H. Loading rate effect on the creep behavior of metallic glassy films and its correlation with the shear transformation zone. *Mat. Sci. Eng. A* **2015**, *622*, 76–81. [[CrossRef](#)]
- Yoo, B.G.; Kim, J.Y.; Kim, Y.J.; Choi, I.C.; Shim, S.; Tsui, T.Y.; Jang, J.I. Increased time-dependent room temperature plasticity in metallic glass nanopillars and its size-dependency. *Int. J. Plasticity* **2012**, *37*, 108–118. [[CrossRef](#)]

18. Wang, Y.; Zhang, J.; Wu, K.; Liu, G.; Kiener, D.; Sun, J. Nanoindentation creep behavior of Cu–Zr metallic glass films. *Mater. Res. Lett* **2018**, *6*, 22–28. [[CrossRef](#)]
19. Ma, Y.; Peng, G.J.; Jiang, W.F.; Chen, H.; Zhang, T.H. Nanoindentation study on shear transformation zone in a Cu-Zr-Al metallic glassy film with different thickness. *J. Non-Cryst. Solids* **2016**, *442*, 67–72. [[CrossRef](#)]
20. Ma, Y.; Ye, J.H.; Peng, G.J.; Zhang, T.H. Nanoindentation study of size effect on shear transformation zone size in a Ni–Nb metallic glass. *Mat. Sci. Eng. A* **2015**, *627*, 153–160. [[CrossRef](#)]
21. Yoo, B.G.; Oh, J.H.; Kim, Y.J.; Park, K.W.; Lee, J.C.; Jang, J.I. Nanoindentation analysis of time-dependent deformation in as-cast and annealed Cu–Zr bulk metallic glass. *Intermetallics* **2010**, *18*, 1898–1901. [[CrossRef](#)]
22. Wang, F.; Li, J.M.; Huang, P.; Wang, W.L.; Lu, T.J.; Xu, K.W. Nanoscale creep deformation in Zr-based metallic glass. *Intermetallics* **2013**, *38*, 156–160. [[CrossRef](#)]
23. Ma, Y.; Peng, G.J.; Feng, Y.H.; Zhang, T.H. Nanoindentation investigation on the creep mechanism in metallic glassy films. *Mat. Sci. Eng. A* **2016**, *651*, 548–555. [[CrossRef](#)]
24. Yoo, B.G.; Kim, K.S.; Oh, J.H.; Ramamurty, U.; Jang, J.I. Room temperature creep in amorphous alloys: Influence of initial strain and free volume. *Scr. Mater.* **2010**, *63*, 1205–1208. [[CrossRef](#)]
25. Bei, H.; Lu, Z.P.; George, E.P. Theoretical strength and the onset of plasticity in bulk metallic glasses investigated by nanoindentation with a spherical indenter. *Phys. Rev. Lett.* **2004**, *93*, 125504. [[CrossRef](#)] [[PubMed](#)]
26. Johnson, K.L. *Contact Mechanics*; Cambridge University Press: Cambridge, UK, 1987.
27. Jiang, Q.K.; Wang, X.D.; Nie, X.P.; Zhang, G.Q.; Ma, H.; Fecht, H.-J.; Bendnarcik, J.; Franz, H.; Liu, Y.G.; Cao, Q.P.; et al. Zr–(Cu,Ag)–Al bulk metallic glasses. *Acta Mater.* **2008**, *56*, 1785–1796. [[CrossRef](#)]
28. Packard, C.E.; Homer, E.R.; Al-Aqeeli, N.; Schuh, C.A. Cyclic hardening of metallic glasses under Hertzian contacts: Experiments and STZ dynamics simulations. *Philos. Mag.* **2010**, *90*, 1373–1390. [[CrossRef](#)]
29. Packard, C.E.; Schuh, C.A. Initiation of shear bands near a stress concentration in metallic glass. *Acta Mater.* **2007**, *55*, 5348–5358. [[CrossRef](#)]
30. Tabor, D. The hardness of solids. *Rev. Phys. Technol.* **1970**, *1*, 145–179. [[CrossRef](#)]
31. Su, C.; Herbert, E.G.; Sohn, S.; LaManna, J.A.; Oliver, W.C.; Pharr, G.M. Measurement of power-law creep parameters by instrumented indentation methods. *J. Mech. Phys. Solids* **2012**, *61*, 517–536. [[CrossRef](#)]



© 2019 by the authors. Licensee MDPI, Basel, Switzerland. This article is an open access article distributed under the terms and conditions of the Creative Commons Attribution (CC BY) license (<http://creativecommons.org/licenses/by/4.0/>).